Developing Auto-Focusing Microscopy For Ultra High-Throughput Biodosimetry

Nina Bahar

Mentor: Dr. Guy Garty

Center For High-Throughput Minimally-Invasive Radiation Biodosimetry

Radiological Research Accelerator Facility

August 7, 2009

Abstract

As part of the National Science Foundation's Research Experiences for Undergraduates program, I was able to come to Columbia University's Nevis Labs to create and work with auto-focusing, imaging, and image processing mechanisms using C and Visual Basic. My project is highly useful for ultra high-throughput radiation biodosimetry assays because of the fast rate at which the system can auto-focus and grab fluorescent images. This paper seeks to capture the important things that I have learned and developed at Nevis.

I: INTRODUCTION

Radiation biodosimetry is defined as the use of biological markers to determine the dose of absorbed, ionizing radiation received by a given subject or sample. The intention of developing a rapid radiation biodosimetry system is that should a radiological incident occur, particularly in a highly populated area, large amounts of people will need to be examined in a short period of time to determine whether or not medical treatment is necessary.

Recent history has lent us a litany of civilian radiological incidents that could have benefitted from this project. For example, from 1982-1984 radioactive steel was scavenged from a reactor and melted into rebar. It was then used to construct apartment buildings in northern Taiwan, exposing 10,000 people to radiation. (Yu-Tzu 2001) In 1983 a resident of Mexico salvaged a radiation therapy machine that still contained 6,000 pellets of Cobalt-60. When his truck was scrapped, it became 5,000 metric tons of steel with an approximated activity of 300 Ci. This was then sold as kitchen/restaurant table legs and building materials, some of which were set to go to Los Alamos National Laboratory. The steel's radioactivity was discovered when the delivery truck accidentally drove through a radiation monitoring station. When the cause of radiation was traced back to the original owner, the area where he drove was scanned and pellets were found embedded in the roadway, leading to many evacuations and investigations. While only a few individuals experienced severe radiation from this incident, 109 houses were condemned.(Combs 1998) Another scrap metal incident occurred when radioactive sources were taken from an abandoned hospital in Goiania, Brazil and were exposed in an urban region of Brazil (population was approximately 1.2 million people in the 1980's) as they made their way through several scrap dealers. When the scrap metal was determined to be dangerous, 112,000 people were examined for radiation with Geiger-counters. Because Geiger-counters detect contamination rather than exposure, they are not of great use medically. (International Atomic Energy Agency 1988) Our project presents a much more efficient approach to examination and triage should any major future incident occur.

Presently high-throughput refers to assessing hundreds of samples per day (24 hours). This project strives to exceed this by two orders of magnitude—to assess 30,000 samples per day (about 19 individual samples per minute). The accomplishment of this goal requires an efficient automated mechanism for transferring and treating samples for analysis, a way to image the samples through automated microscopes, and effective imaging software to process the images once they are obtained.

II: The Transfer and Treatment of Samples

Assays With The Rapid Automated Biodosimetry Tool (RABIT)

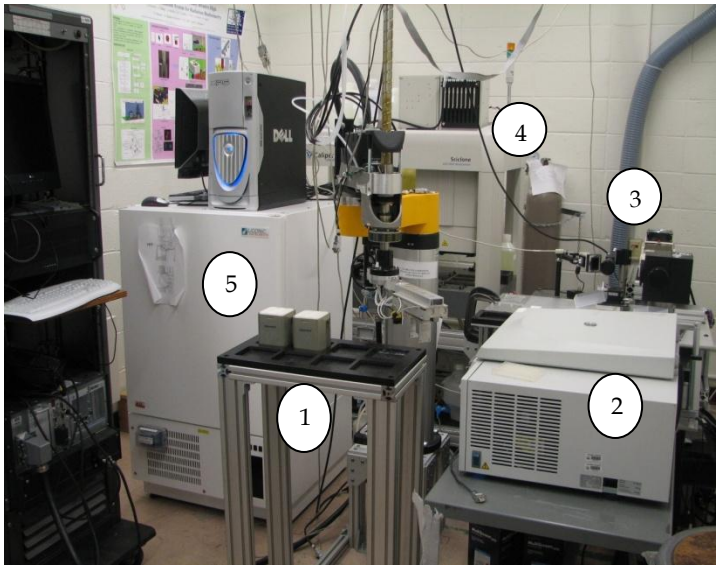

1-Input stage

2-Centrifuge

3-Cell harvesting module

4-Liquid/plate handling

5-Incubator

Figure 1

The RABIT (Figure 1) begins with the input stage. Finger-stick samples of blood are transferred into PVC capillaries that sit in the buckets on the input stage. The four 96-slot buckets are placed into the centrifuge and spun at 4,000 rpm for five minutes, producing a small band of pure white blood cells. Next, the buckets are removed from the centrifuge and the cell harvesting module's capillary grabber pulls out the capillaries. The capillaries have their patient identification barcodes checked by a reader and are then held in front of an ultra-violet (UV) laser so that they can be cut—making the white blood cells easier to extract. In order to determine the cut line, an image is taken of the capillary and, through image processing controls, the laser is told to cut 40 mm away from the white blood cell cluster, between the red blood cell and white blood cell bands. This also separates and discards the part of the tube with the red blood cells. Air pressure is then applied to the capillary, pushing the lymphocytes into the appropriate well in a 96-well plate. It is important to emphasize that the microwells are filter-bottomed because reagents can be removed and replaced without having to resubmit the lymphocytes to centrifuging. The plates are then taken to the liquid handling station. Because the specifics of the liquid handling are assay-dependent, the liquid handling details are included within the assay descriptions.

Micronucleus Assay

To understand the micronucleus assay, one must first have a basic knowledge of cell division, to which a brief paragraph will be devoted.

During interphase a cell saves up energy, DNA has already replicated and waits in a loosely bound bundle (chromatin). Prophase and prometaphase establish structures of motion within the cell—DNA coils into chromosomes consisting of two chromatids bound by a centromere. Protein structures called kinetochore form on the centromeres as centrioles polarize to the ends of the cell. The nuclear membrane surrounding the DNA disintegrates. Metaphase consists of spindle fibers extending from the centrioles to the kinetochore and orienting the chromosomes along the center of the cell. In anaphase the spindle fibers retract, pulling the chromosomes apart at the centromeres and bringing the sister chromatids to the poles of the cell; in telophase, nuclear envelopes reform around the newly divided chromatids and the cell undergoes a division in its membrane. Two new cells with identical DNA are formed.

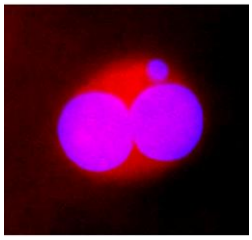

Figure 2

When cells are irradiated, DNA is broken. DNA fragments that do not join to a centromere will not be re-oriented metaphase and anaphase. When telophase occurs, pieces of chromosome that do not become part of either daughter nuclei form their own nucleus to the side of the daughter nuclei. This is illustrated in Figure 2's binucleate cell in which the nuclei are colored pink. For the micronucleus assay, blocking chemicals are added to prevent cytokinesis. Only binuclear cells are studied for micronuclei because it is clear that they've progressed to telophase in cell division.

The micronucleus assay can observe radiation in lymphocytes, provided they are chemically induced to undergo cell division. Combining said induction with the amount of time required for cell division to take place yields a 72 hour processing time. For the micronucleus assay, the liquid handling station removes plasma by applying pressure, washes the samples twice with phosphate buffered saline (PBS) to remove blood plasma and chemicals which may inhibit cell division, and puts the cells in a medium that contains stimulants for cell division (phytohemagglutinin/PHA). After 48 hours the medium is renewed and Cytochalasin B (Cyt B) is added to stop the cell membrane from dividing. After 28 hours the liquid handling apparatus removes the medium, washes the samples with PBS, and adds frigid Methanol as a fixative to leave in for ten minutes. Once the fixative is removed and the cells are dry, the apparatus stains the cells with CellMask™ Orange and DAPI. The cells are washed three more times with PBS and a signal is sent to RABIT to put the cells into the incubator.

Micronuclei are observable for years after exposure, making this assay an excellent option for patients whose samples are treated anytime after 36 hours of exposure. For immediate triage there is a second, faster assay that detects a damage signal present during the first 36 hours post-exposure.

The γ-H2A-X assay

H2A-X, a member of the H2A histone family, plays a significant role in the organization and repair of chromatin. When DNA undergoes radiation damage, it breaks and large amounts of γ-phosphorylated H2A-X form foci around the site of the double strand breaks in attempt to help repair DNA. Because the presence of phosphorylated H2A-X is dependent upon the DNA repair process, it is only observed within 36 hours of radiation exposure. With the γ-H2A-X processing times at a few hours, it is ideal for analysis within 36 hours of exposure.

Like the micronucleus assay, the γ-H2A-X assay begins with lymphocyte capture and plasma removal through the use of positive pressure to flow plasma through the filter-bottoms of the wells. The cells are washed twice with PBS and then frigid Methanol is added again as a fixative. Ten minutes later, this is removed and 2% Bovine serum albumin is added as a blocking medium. After half-an-hour the primary antibody that targets γ-H2A-X is added and half-an-hour after that the second antibody that carries the fluorophore Alexa Fluor 555 is added so that it can bind to the first antibody, making the sites of double strand breaks visible through the use of fluorescent microscopy. (Figure 3) After another 30 minutes the cells are washed three times with PBS, stained with DAPI, and washed again with PBS. What is so fascinating about this assay is that it enables one to see what is happening on the genetic level (through the presence of foci) without an exceedingly powerful microscope.

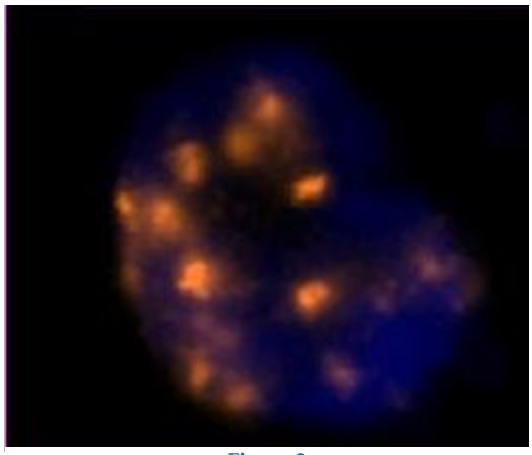

Figure 3

Biodosimetric Applicability

Previous study has confirmed that both assays are strong candidates for dosimetric purposes. (Amundson 2001) The amount of micronuclei per cell relates quadratically to the radiation dosage (Figure 4) and the amount of γ-H2A-X foci/ total fluorescence of the γ-H2A-X foci relates linearly to the dose of radiation. (Figure 5)

Figure 4

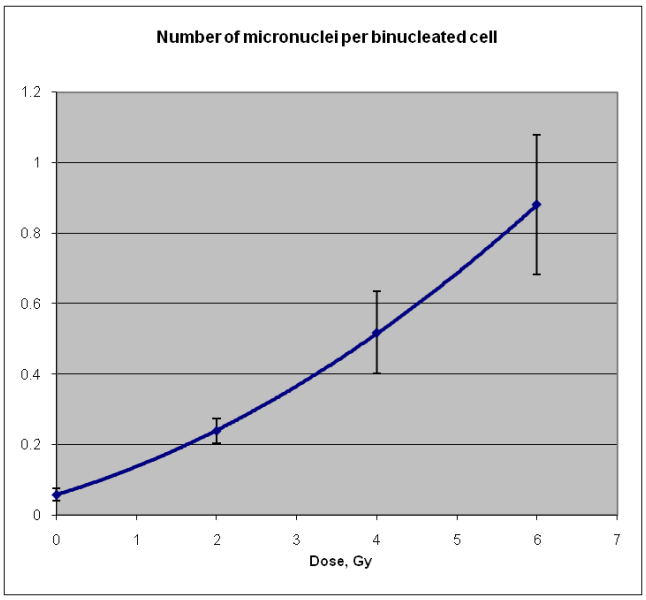

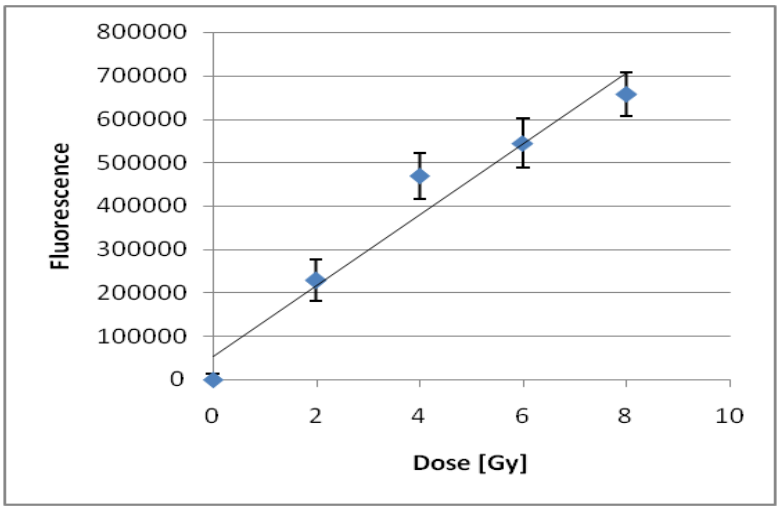

Figure 5, Fluorescence of γ-H2A-X Foci

III: IMAGING

FLUORESCENT IMAGING

From the images of the micronuclei and the γ-H2A-X foci (Figures 2 & 3) it is apparent that advanced imaging and microscopy techniques are indispensable. So as to understand how this project's imaging system is designed, one should first review the basic principles of fluorescence.

The stains used in fluorescence imaging are called fluorochromes (when fluorochromes are manually added to the sample at hand they are called

fluorophores). As exhibited with the antibodies in the γ-H2A-X liquid handling procedure, they bind to certain biological structures depending on observational intent. Fluorescence occurs when electrons within a sample are excited by certain wavelengths of light. As the sample's excited electrons return to ground state, its emission spectrum shifts to higher wavelengths, making it easier to distinguish emission from absorption light when setting up light filters. This phenomenon is called Stokes' Shift. Filter setup is challenging because oftentimes the absorption and emission spectra overlap in between their peaks; if one does not pass and/or receive light far enough from the overlap, there will be a lot of background in the image. Getting too far from the peaks, however, would require longer frame grabbing times and would therefore limit throughput. A visual representation of this is provided by Nikon MicroscopyU. (Figure 6)

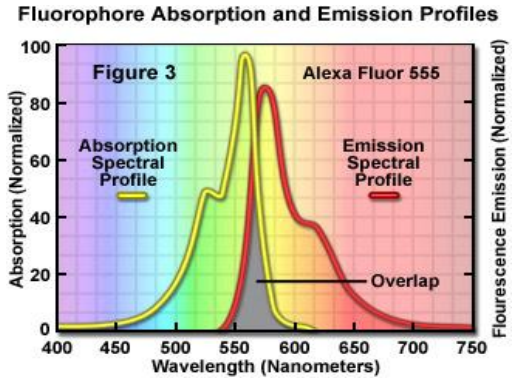

Figure 6, For the γ- H2A-X foci, we use Alexa Fluor 555 to absorb green and emit orange.

Fluorescent-Filtration Microscopy

In order to have a microscope that transmits and reflects what is necessitated to produce a high-quality fluorescent image, specially coated filters called dichroic beam-splitters are needed. They are designed to distinctively transmit and reflect certain wavelengths. In most typical setups, source light is sent through an excitation filter that allows light that will be absorbed by the sample to pass. This light is reflected off of a dichroic beam-splitter and sent through the sample. The beam-splitter will transmit the ensuing emission light to the appropriate destination.

The system specific to this project (Figures 7, 8, & 9) utilizes four dichroic beam-splitters.

Figure 7

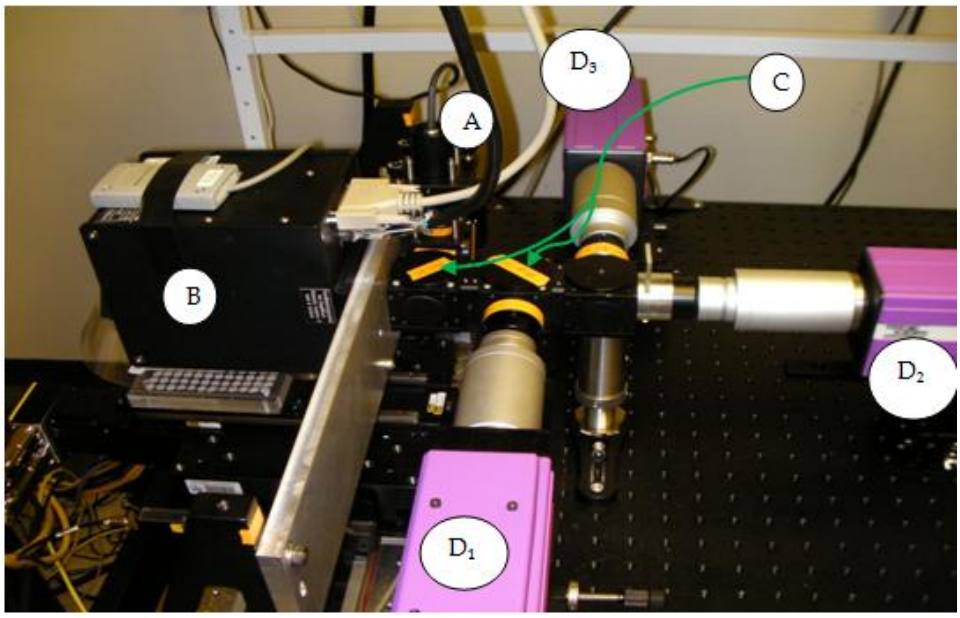

A: Source light, B: Scan head, C: Beam-splitters, $D_{1, 2, 3}$: Intensifiers with attached cameras (not pictured)

Figure 8

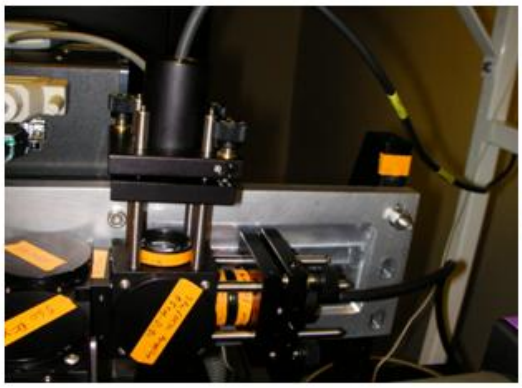

The source light entry

Figure 9

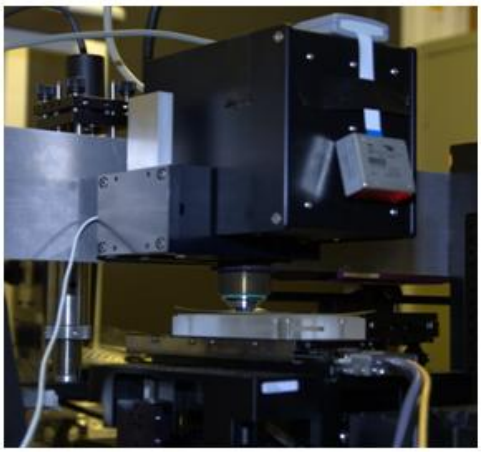

The scan head, stage, and objective

The path of the light through the system (best followed through Figure 7) is as follows: the green and UV source light (close-up Figure 8) are merged by one beamsplitter and then reflected by another dichroic beam-splitter so that the light goes to the sample on the observation stage. The sample's electrons are excited and emit orange light from the green absorption and blue light from the UV absorption. The orange light is transmitted through both dichroics and sent

to intensifiers $D_{2,3}$ after being split by a third beamsplitter, while the blue light is transmitted through the source-reflecting dichroic (the leftmost dichroic in Figure 7) and reflected off of the orange-transmitting dichroic so that it is sent to intensifier D_1. The light is sent to three intensifiers (with attached cameras) because each assay requires three types of images per sample. In the case of micronuclei, the D_1 intensifier receives the image of the nuclei and micronuclei in the binuclear cells. The D_2 intensifier is used for focusing the sample and the D_3 intensifier is used for imaging the cytoplasm. Combining these images produces a superb final image with relevant parts of the cell distinctly visible. With the γ-H2A-X assay, D_1 is for the foci, D_2 is for focusing, and D_3 is for the nuclear membrane.

In discussing the automated components of the microscopy system, I'll begin with the scan head apparatus (Figure 9). The scan head consists of an objective attached to a piezo-electric stage that can conduct fine focusing as it moves on a 100-micron scale. The scan head's objective is over the parker stage, where the sample sits. The parker stage moves in all directions and is excellent for coarse focusing as its smallest motion increment is 0.01 mm. Both stages' controls are coded in C. The user is able to give the control program a direction of motion followed by a unit of motion and that—through the use of Recommended Standard 232 (RS-232)—moves the parker stage accordingly. For focusing with the piezo-stage, one can provide the direction and magnitude of focus which generates a voltage that corresponds to a given piezo-electric orientation. The gain on the image intensifiers as well as the ability to display streaming video and take snapshots with the cameras is controlled by the program as well. There is another interface written in Visual Basic that can process the images and find the parameters necessary for making biodosimetric conclusions.

IV: AUTO-FOCUSING

When a sample is out-of-focus in a spherical lens system the resulting microscope image is blurry. It would be difficult to auto-focus the system based off of this out-of-focus image because spherical blurriness is not straightforward to quantify. The system has no way of knowing whether or not the piezo-electric stage needs to move up or down to yield a focused image because above and below focus images look the same. Spherical lenses cannot be used to determine if an out-of-focus sample is above or below focus because the images for both cases have the same properties. This problem is solved by adding a weak cylindrical lens to the system.

Named for the shape of their surface, cylindrical lenses focus to lines instead of to points (what spherical lenses focus). Cylindrical lenses are able to do this because they are more curved around one axis than around another axis. Figure 10 is a ray optics diagram that shows how this impacts the resultant image.

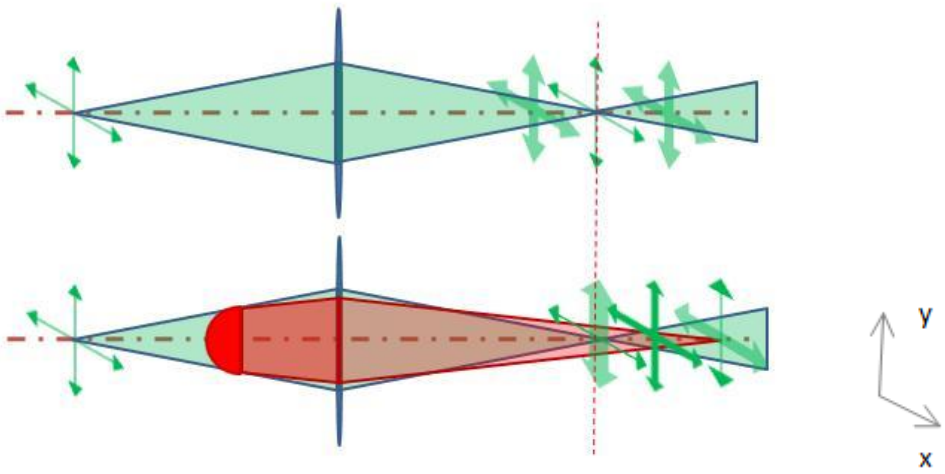

Figure 10

The upper system in Figure 10 contains a simple spherical lens and is used by this project for the $D_{1,3}$ imaging intensifiers. The lower system has a cylindrical lens added to the spherical lens, producing an image that is dominant on one axis above focus and dominant on another perpendicular axis below focus. If one is looking through the cylindrical system in Figure 10, a circular sample from above focus (objective is too close to sample) will appear elliptical along the x-axis and from below focus (objective too far from sample) will appear elliptical on the y-axis. For the samples that we're analyzing, being above and below focus is a matter of microns. The filter leading to the D_2 intensifier is outfitted with a cylindrical lens. (Figure 11)

Figure 11

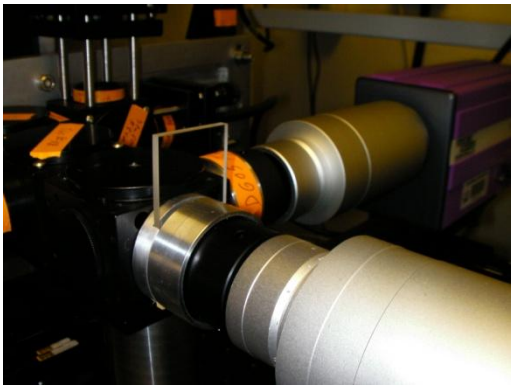

The system will be considered in focus when the D_2 intensifier yields a circle instead of an ellipse. As shown in Figure 10, the point in space at which the cylindrical system attains a 1:1 aspect ratio occurs slightly farther away from the original focal point, which is where spherical lenses yield a focused image. To compensate for this fact the positions of both of the intensifiers and their corresponding cameras can be easily adjusted. Specifically, the D_2 intensifier and camera are slightly farther from the system than the $D_{1,\ 3}$ intensifiers and cameras. This arrangement can be easy to achieve with a known test sample. Once the setup is aligned and adjusted, its output images must be processed and analyzed to get aspect ratios used for auto-focusing.

When the imaging code is fully developed, the system will be able to grab a single image and, based on its aspect ratio, will be able to move the piezo-electric stage to the appropriate position to yield a focused image based on the aspect-ratio to position relation presented in my data. The aspect ratio (x-length/y-length) for an object above focus in Figure 10 would be less than 1 and for an object below focus the ratio would be greater than 1. Image analysis controls are utilized to find the aspect ratio, but images must be preprocessed before they are analyzed to yield satisfactory results.

PREPROCESSING

The two main methods of pre-processing utilized in the Visual Basic interface are rank filters and background subtraction. Background subtraction is performed by capturing an image while the system is in operation but no bead is in the objective and subtracting said image from all of the bead images prior to analysis. This removes background glare around particles and increases the image's clarity. A rank filter works by defining a center set of pixels based on locations with the highest pixel gradients. The pixels around this center set are ranked by the rank filter, creating an overall function for the region around the center set of pixels. It then uses this function to create new values for the center set, essentially removing hot-pixels. (Figure 12)

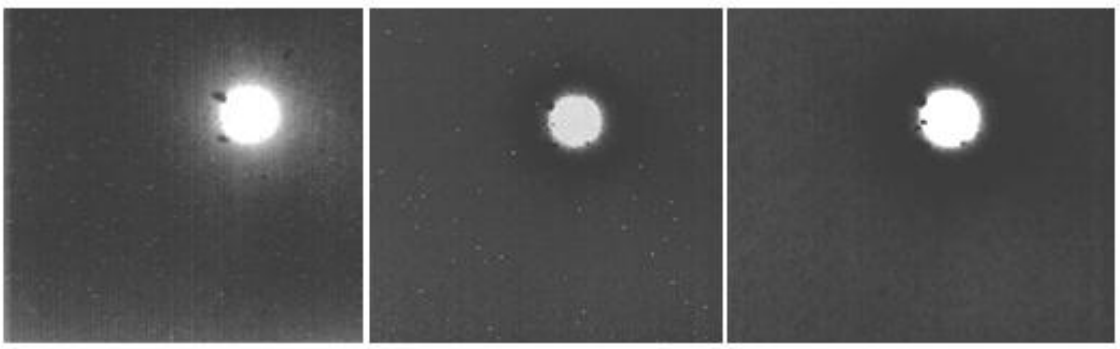

Figure 12, Original image (left), Step 1: Background subtracted (center), Step 2: Rank filter applied (right)

Preprocessing is very important because too much background or hot-pixel-presence could invalidate the image processing calculations, making the images unusable for biodosimetry.

PROCESSING

Once a clean image is attained it is then processed for aspect ratios. Feret analysis can be used to determine the aspect ratio of a sample. The Feret diameter is defined as the perpendicular distance between parallel tangents of a particle (profile perpendicular to the objective). Objects have several Feret diameters that are taken at a defined number of angles (in this case at least 12) between 0° and 180°; the longest of said diameters is selected as the result. Dividing the maximum Feret diameters along the x and y-axes yields an aspect ratio.

Another method of calculating the aspect ratio is auto correlation. Technically, auto correlation is the cross correlation of a function with itself. In simple terms, the image processing code takes an image, shifts it along one axis (either x or y), multiplies the shifted image by the original non-shifted image, and sums the pixel values. This process is then repeated with a shift along the axis that was not shifted the first time, and the results of both auto correlations are then divided to yield an aspect ratio. Mathematically this procedure is expressed in Equation 1 where I(x, y) is the pixel value at a given point and δ is the shift factor for the given axis. Because auto correlation relies on the total fluorescence of the image, it is dependable for single beads, but for multiple beads Feret analysis gave the best results. When both methods of analysis are used on a single bead they have reproduced very close aspect ratios. More data must be compared between both methods, however, before a definitive statistical conclusion can be made.

$$\frac{\int\int dx\, dy\, I(x, y) \cdot I(x - \delta_x, y)}{\int\int dx\, dy\, I(x, y) \cdot I(x, y - \delta_y)}$$

Equation 1

V: DATA

Once the stage-moving and image processing code was running, the opportunity to take data presented itself. In taking data I chose to use fluorescent spherical beads because they are close to lymphocyte size and shape and they will be seeded in with the lymphocyte samples for calibrating the focus of the imaging system. With code that moved the piezo-electric stage through a range of positions I was able to capture excellent images. (Figure 13)

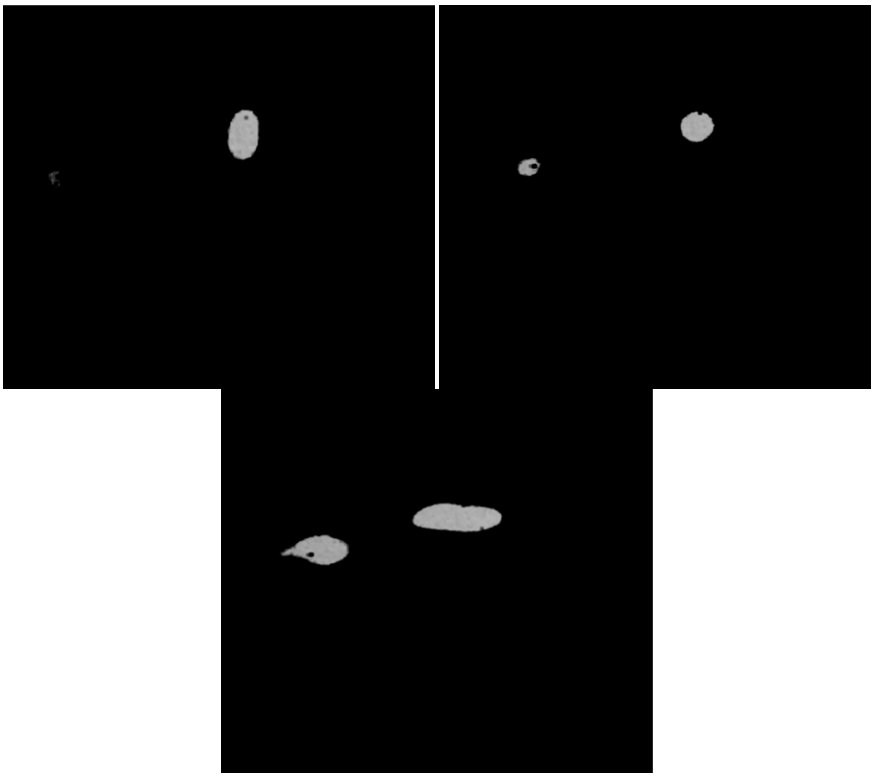

Figure 13

The upper-left and bottom images are clearly oblong on different perpendicular axes while the upper-right image is essentially circular, as expected.

In gathering aspect ratios and plotting them against the distance between the objective and the sample, we expected our results to be similar to the plano-concave simulation shown in Figure 14. Because the piezo-electric stage is scanning a smaller range it was expected that our data would be similar to that which is between the plano-concave peaks where the relation follows a third order polynomial.

Figure 14

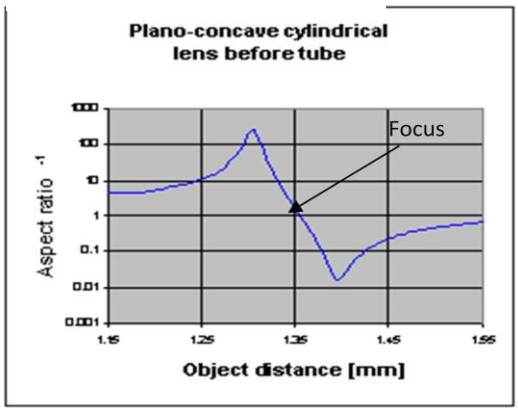

And that is exactly what we found (Figure 15); with chi-squared (or R^2) values of 0.9945 for the cylindrical lens with focal length 700 mm and 0.9994 for the cylindrical lens with focal length 1000 mm, the data fit a third-order polynomial.

Figure 15

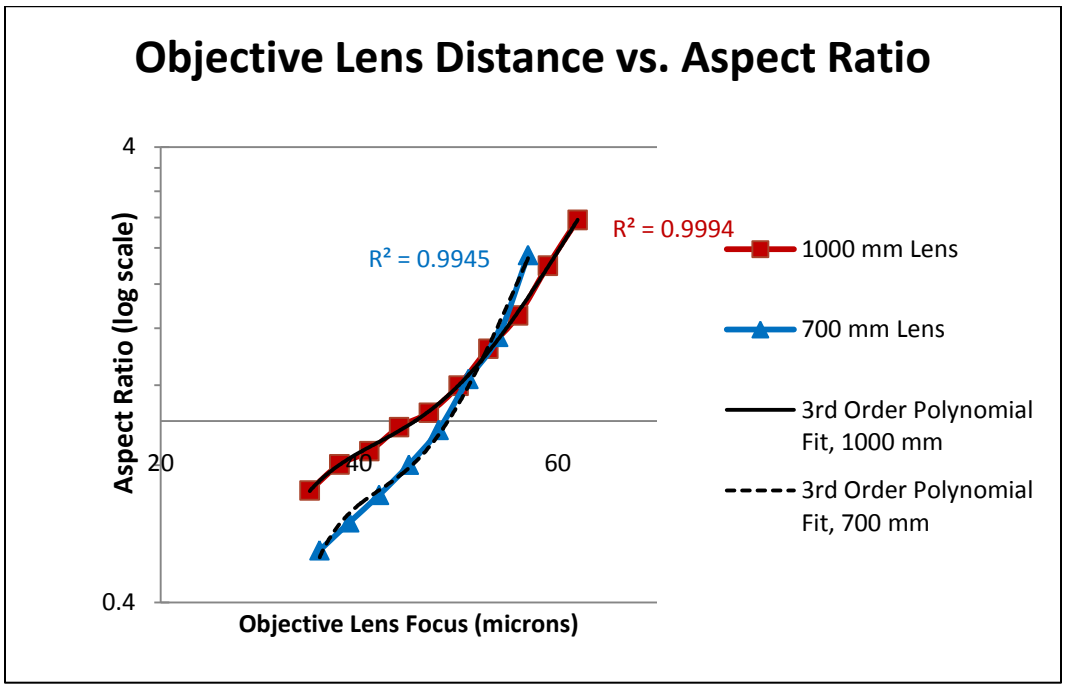

With these polynomial relations between position and lens focus (in the form of piezo-electric stage position), we expect to have the system capable of auto-focusing after just one image grab to determine whether the lens is above or below focus.

VI: Conclusions

- An ultra high-throughput means of biodosimetry is necessitous for triage following radiological incidents, especially in heavily populated areas.
- A rapidly processing and focusing system is vital to achieving ultra high-throughput status.
- Using cylindrical lenses we can determine how to focus the system using a single image.
- My imaging system tested on beads will be able to perform the focusing required to image the lymphocytes reliably.

VII: Acknowledgements

While working at Columbia University's Nevis Labs I learned a lot of important things. I learned that—whether in the form of a birthday cake, soldering damage control, or a chance to see an accelerator get taken apart—the

people at the Radiological Research Accelerator Facility are always ready to provide seriously nontrivial amounts of support and encouragement to their summer students. Everyone at RARAF and at Nevis as a whole made me feel embedded in the community, making this summer a memorable experience.

Specifically I would like to thank my mentor, Dr. Guy Garty, for all that he has shown and taught me; Professor David Brenner, the director of the Center for Radiological Research; Dr. Gerhard Randers-Pehrson, the chief physicist at RARAF; Mr. Steve Marino, the RARAF manager; the National Institutes of Allergy and Infectious Diseases, for funding this project (NIAID grant U19 AI067773); and the National Science Foundation, for creating and maintaining Research Experiences for Undergraduates.

REFERENCES

Amundson S A, Bittner M, Meltzer P, Trent J and Fornace A J J. 2001. "Biological indicators for the identification of ionizing radiation exposure in humans." *Expert Rev. Mol. Diagn.* **1** 211-9

Combs, Susan. "El Cobalto". Bordering the Future. Texas Controller of Public Accounts. July 1998.

International Atomic Energy Agency. *The radiological accident at Goiânia.* (1988)

Spring, Kenneth R. and Michael W. Davidson. "Introduction to Fluorescence Microscopy." Nikon MicroscopyU. http://microscopyu.com/articles/fluorescence/fluorescenceintro.html. Figure 3.

Yu-Tzu, Chiu. "Radioactive Rebar linked to Cancer." *The Tapei Times*. 29 April 2001: p. 2.